Proximity effect: Amorphous Sn-Fe, amorphous Bi-Fe films

G. Cort* and D. G. Naugle
Department of Physics, Texas A&M University, College Station, Texas 77843
(Received 25 August 1980)

We report the results of an experimental investigation of the proximity effect in sandwiches of amorphous Bi-Fe and amorphous Sn-Fe. The measurements on *a*-Bi films resolve a controversy concerning its coherence length while that derived for *a*-Sn is consistent with values reported from critical-field measurements. The pair penetration depths determined from a new analysis technique are consistent with values derived from other proximity experiments which employ Fe normal layers. A linear decrease of the transition temperature with resistance per square and inverse film thickness, an apparently universal characteristic of amorphous superconducting films, was also observed in these experiments.

I. INTRODUCTION

The proximity effect on a superconductor in intimate contact with a ferromagnetic normal metal has been studied by several authors.[1–5] These experiments are characterized by very strong proximity effects due to strong pair breaking by the ferromagnetic domains of the normal metal. Hauser *et al.*[1,6] and Kircher[2] have demonstrated this for gadolinium, iron, and nickel normal layers.

Hauser *et al.*[1] (HTW) have extended the de Gennes-Werthamer theory of proximity effects[7,8] to include sandwiches with ferromagnetic normal-metal layers by the inclusion of the average lifetime, τ, of a Cooper pair inside the ferromagnetic material which can be expressed in terms of the de Gennes[9] extrapolation length b. In addition to this parameter, the theory is described in terms of microscopic parameters peculiar to both the normal-metal layer and the superconductor. Fortunately, the theory is not particularly sensitive to the normal-metal parameters, at least in the thick-film limit; consequently, Lejeune and Naugle[5] have suggested that the proximity effect with ferromagnetic normal-metal layers can provide a simple method which does not require a magnetic field to measure the coherence length of the superconductor, $\bar{\xi}_S$.

Most experiments with the proximity effect have relied on the calculation of $\bar{\xi}_S$ from measured normal-state properties and used b as the parameter to be fitted to the data. For the amorphous superconducting films many normal-state properties, in particular, the specific heat, have not been measured. Lejeune and Naugle assumed $b=0$ and fitted the data to determine $\bar{\xi}_S$. Their value of $\bar{\xi}_S = 60$ Å for amorphous Bi films agreed well with an independent determination based on paraconductance measurements ($\bar{\xi}_S = 63$ Å) by Silverman,[10] but these values disagreed with the coherence length calculated from paraconductance measurements with a perpendicular magnetic field by Silverman[11] ($\bar{\xi}_S = 46$ Å) and upper critical field measurements, $H_{c2}(T)$, by Bergmann[12] ($\bar{\xi}_S = 44$ Å). The larger values were determined from experiments which require accurate knowledge of the film thickness whereas the latter results are independent of thickness measurements but require a perpendicular magnetic field.

Three possibilities to explain the two different values of $\bar{\xi}_S$ from the four experiments are apparent. The most obvious is that the thicknesses measured for the two experiments were in error and that their agreement was fortuitous. Silverman[11] has suggested that expansion of the *a*-Bi films on crystallization to the semimetal phase which occurs before film thickness measurements can be made would lead to consistently larger measured values of thickness than actually exists for the amorphous films. A third possibility is that the coherence length could depend on magnetic field which would give two values, one for experiments which need a magnetic field and another for those in zero field.

We report proximity effect experiments between *a*-Bi and *a*-Sn superconducting films and Fe overlayers. Particular care was taken in film thickness determinations and in the analysis the data was weighted according to thickness measurement uncertainties. Amorphous Sn was chosen because the density change of Sn on melting is small and therefore thickness measurements after crystallization should differ only slightly from the true thickness of the amorphous Sn. An improved fitting procedure was used which allowed determinations of both the parameters $\bar{\xi}_S$ and b and the results were compared with determinations of $\bar{\xi}_S$ for these two materials based on independent experiments. We believe that these results resolve the controversy on the value of $\bar{\xi}_S$ for *a*-Bi and demonstrate that indeed accurate values of $\bar{\xi}_S$ may be obtained from proximity effect measurements. Additionally the thickness dependence of T_c for *a*-Sn films is reported.

II. SUMMARY OF THE HTW THEORY

The HTW theory of the proximity effect between a superconductor and a ferromagnetic metal is an extension of the formulation of Werthamer.[8] For sandwiches with nonmagnetic normal components, the transition temperature of a proximity sandwich is given by four equations:

$$\chi(\xi_S^2 k_S^2) = \ln(T_{cS}/T_c) \ , \tag{1}$$

$$\chi(-\xi_N^2 k_N^2) = \ln(T_{cN}/T_c) \ , \tag{2}$$

$$\sigma_S k_S \tan(k_S D_S) = \sigma_N k_N \tanh(k_N D_N) \ , \tag{3}$$

$$\chi(y) = \psi(\tfrac{1}{2} + \tfrac{1}{2}y) - \psi(\tfrac{1}{2}) \ , \tag{4}$$

where T_{cS} and T_{cN} are the transition temperatures of the superconductor (S) and the normal metal (N), respectively, D_S and D_N are the thicknesses of the individual sandwich components, σ_S and σ_N are the normal-state conductivities of each sandwich component, and the subscripts S and N refer to the superconducting and normal sandwich components, respectively. Additionally, $\psi(y)$ is the digamma function defined and tabulated in Ref. 13, and the coherence lengths $\xi_{N,S}$ are defined by the relation

$$\xi_{N,S}^2 = (\hbar v_F l/6\pi k_B)_{N,S} T_c^{-1} \ , \tag{5}$$

where $\hbar$ is Planck's constant (divided by 2π), k_B is Boltzmann's constant, v_F is the Fermi velocity, and l is the mean-free path of electrons.

Hauser *et al.*[1] effectively extended these equations to apply to ferromagnetic N layers by replacing Eq. (2) with the expression

$$\chi(-\xi_N^2 k_N^2 + \alpha/t) = \ln(T_{cN}/T_c) \ , \tag{6}$$

where $\alpha = \hbar/2\pi\tau k_B T_{cS}$. Here τ is the effective spin-scattering lifetime of a Cooper pair in the N material and $t = T_c/T_{cS}$. Equations (1) and (3)–(6) then express the HTW theory.

As shown by Hauser and co-workers,[6] the role of the parameter τ can be equivalently expressed in terms of the de Gennes extrapolation length $b = [d \ln\Delta/dz]^{-1}$ at the N-S interface. With the explicit solution[8] for $\Delta(r)$, Eq. (3) can be solved (in the limit $k_N D_N >> 1$) to give

$$k_N^{-1} = \rho_S b/\rho_N \ , \tag{7}$$

where $\rho = 1/\sigma$. In addition, if the χ function is approximated by the expression[8]

$$\chi(y) = \tfrac{1}{4}\pi^2 \ln(1+y), \quad -1 < y \leq 0 \tag{8}$$

and if $\alpha >> 1$ and $T_{cN} = 0$, then the depth of penetration of Cooper pairs into the normal material is

$$k_N^{-1} = (\tau v_F l/3)_N^{1/2} \ , \tag{9}$$

which depends only on the electronic properties of the normal component. Finally, if $D_S >> b$, it follows that

$$k_S = \pi/2(D_S + b) \ . \tag{10}$$

This allows Eqs. (1), (3), and (6) to be replaced by the single expression

$$\chi\left(\frac{\pi^2 \xi_S^2}{4(D_S+b)^2}\right) = \ln(T_{cS}/T_c) \ , \tag{11}$$

which describes the general case in which Cooper pairs diffuse across the N-S interface and remain correlated for some short distance into the ferromagnetic metal. The effect of the magnetic nature of the N component is expressed in Eq. (11) through the dependence on the extrapolation length b. As Hauser *et al.*[6] have pointed out, however, k_N^{-1}, not b, is the appropriate measure of the depth of penetration of Cooper pairs into the N metal.

III. EXPERIMENTAL DETAILS

The features of the apparatus and most of the procedures employed are dictated by the stringent conditions which must be met in order to successfully measure the properties of proximity sandwiches. Most importantly, the N-S interface must be kept free of interlayer oxidation as such an insulating layer between the sandwich components decouples the films and suppresses the proximity effect. It is also important to limit interlayer diffusion, as this process also suppresses the proximity effect.[14]

Measurements were performed in the high-vacuum, cold-finger cryostat described in detail by Naugle *et al.*[15] The proximity sandwiches were grown *in situ* on a quartz substrate mounted on a copper block attached to a liquid-helium (LHe) reservoir. The substrate communicates with the evaporation oven through a series of shuttered windows in the surrounding light-tight radiation shields, one at liquid-nitrogen temperature and the two inner at liquid-helium temperature. The shutters can be actuated from outside the cryostat, allowing the substrate to be optically isolated from the remainder of the vacuum chamber by the three cryogenic shields during measurements. Temperature measurements were provided by a calibrated Ge resistance thermometer.

Conventional pumping was provided by a six-inch water-cooled diffusion pump. Considerable cryopumping also occurred due to the cold shields and reservoirs inside the vacuum chamber. The ultimate pressure measured at the outer wall of the vacuum chamber was approximately 10^{-8} torr, although we estimate the residual gas pressure at the substrate to be at least an order of magnitude lower due to differential pumping by the cold shield.

A dual mask system was used to deposit each com-

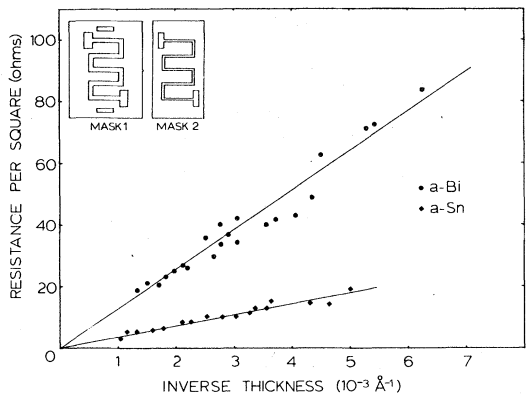

FIG. 1. Residual resistance per square of a-Bi and a-Sn films as a function of inverse thickness. The evaporation masks are shown as an inset.

ponent of the sandwich through a mask of different cross-sectional area. The masks used are shown as an inset in Fig. 1. Mask 1 was fixed directly over the substrate. Mask 2 was mounted in a track in front of mask 1 and aligned so that its horizontal segments were centered over the corresponding segments of mask 1. A latching mechanism was activated from outside the cryostat to engage mask 2 and pull it below the level of the substrate, thereby exposing mask 1. This system allowed the S component of each sandwich to be deposited through the narrow pattern of mask 2, and the N component, through the wider pattern of mask 1.

A large body of data characterizing a-Bi already exists including measurements of transition temperature,[16,17] resistivity,[17] paraconductance,[10,11,18] upper critical field,[12] and penetration depth.[19] Although the data available for a-Sn are not as extensive, sufficient results exist for comparison with this experiment.[12,20–22] Even at the low temperatures at which they are grown (< 10 K), these materials require small concentrations of impurity elements to stabilize the amorphous phase. The bismuth samples measured in this study were alloyed with 3 at.% thallium. Tin samples were alloyed with 14 at.% copper. High purity (99.99%) shot was used as the source material for the alloys. Appropriate weights were mixed and melted under vacuum in a quartz tube. The mixture underwent at least four cycles of melting and agitation to ensure homogeneous alloy composition.

The superconductor was evaporated from a Ta band through both masks and quench condensed in the amorphous phase[16,23] onto the cold (< 10 K) quartz substrate. Deposition rates were 2–4 Å/s. By exposing each segment of the mask at successively later times, five films of different thickness were deposited each run. At the conclusion of the evaporation, all shutters were closed to isolate the film from residual gases in the cryostat.

The ferromagnetic samples consist of 99.99% pure Fe wire evaporated from a W source. The details of the Fe evaporation are similar to above with the exception that only mask 1 is in place. Iron is deposited on the superconductor until the resistance of the sandwich is observed to decrease. This procedure generally yields uniform Fe overlayers with thicknesses in the range from 50 to 100 Å.

Several comments concerning the characteristics of the sandwiches grown in this manner are in order. The alloy composition of the superconducting films is expected to be very nearly that of the original alloys. This is due primarily to the approximately equal vapor pressures of the constituent elements. In addition, surface roughness and interlayer diffusion are both expected to be minimal. The latter mechanism has been reported virtually absent in films which are quench condensed.[1] Surface roughness, however, is determined primarily by the choice of samples. Amorphous superconductors generally exhibit excellent homogeneity and uniformity of growth.[23] This is borne out by the small average thicknesses at which the samples of this study became electrically continuous ($\simeq 30$ Å for a-Bi and $\simeq 45$ Å for a-Sn).

After the S films were deposited, transition curves were recorded for each film on an x-y recorder while both warming and then cooling the film. The transition curve for the first film was repeated after completion of that for the last, approximately thirty minutes after completion of the deposition of the superconducting films, and the Fe overlayer then deposited. Differences between the transition curves of a given film were always less than 0.6 mK.

After deposition of the Fe overlayer, a second set of transitions was measured to characterize the sandwich transition temperatures. The data represented by the two sets of profiles, along with measured values of D_S, completely characterize the proximity effect of each sandwich.

The S component thickness was measured separately for each sandwich using the method of Tolansky.[24] Because each sandwich component was grown through a different mask, the resulting sandwiches were terraced, thereby allowing the thickness of either component to be measured directly at the film site. After removal from the cryostat, the S component of each sandwich was measured five times to determine a reliable average value for D_S. In practice, the uncertainty in these average values was approximately ± 30 Å. In addition, the interference pattern associated with each film was photographed to provide a permanent record of the thickness data and to allow verification of the original thickness measurements from an enlarged print. Thickness measurements made from the photographs generally agreed with those made directly on the films to within ± 20 Å and were subject to the same uncertainties.

IV. RESULTS AND ANALYSIS

A. *S* component characteristics

The residual resistance and transition temperature was measured in order to characterize the *S* component. For comparison between films of different dimensions it is convenient to express resistances in terms of the resistance per square $R_\square$, a normalized quantity defined by

$$R_\square = WR/L = \rho/D_S \ , \tag{12}$$

where L, W, and D_S are the length, width, and thickness, respectively of the superconducting film, ρ is the electrical resistivity and R is the film resistance. Thus, $R_\square$ can be calculated for each film from a knowledge of the film resistance and dimensions.

Figure 1 is a plot of the residual resistance per square of the *S* films as a function of reciprocal thickness. The ratio of film length to width is measured for all of these films to be $12.95 \pm 5\%$. This results in values of $R_\square$ which correspond to $\rho = 1.39 \times 10^{-6}$ Ω m for the *a*-Bi films which may be compared to values of 1.55×10^{-6} Ω m reported by Naugle *et al.*[17] and 1.60×10^{-6} Ω m by Bergmann.[12] The resistivity of *a*-Sn is calculated from this data to be 0.40×10^{-6} Ω m as compared to values of 0.45×10^{-6} Ω m and 0.47×10^{-6} Ω m reported by Korn *et al.*[21] and Bergmann,[12] respectively. The discrepancies between the previously published values of ρ for each of these amorphous superconductors and the values we report here are most likely due to inaccuracies associated with measurements of the thickness of the *S* component of each sandwich. It should also be noted, however, that the *S* films are grown through a mask (mask 2) which is mounted several millimeters above the substrate. This may have resulted in broadening of the edges of the films which contributes to the error in our resistivity determination.

Naugle *et al.*[17] have shown that the transition temperature T_{cS} of most amorphous superconductors is thickness dependent and is described by an equation of the form

$$T_{cS} = T_0 - \tilde{K}'/D_S = T_0 - \tilde{K}R_\square \ , \tag{13}$$

where $\tilde{K}'$, $\tilde{K}$, and T_0 are positive constants. The value of T_0 corresponds to the transition temperature of a bulk (infinitely thick) film, whereas the values of $\tilde{K}'$ and $\tilde{K}$ should remain constant for a given superconductor over a wide range of thickness. Figures 2 and 3 are, respectively, plots of T_{cS} vs D_S^{-1} and T_{cS} vs $R_\square$ for the *a*-Bi and *a*-Sn films. Ten films for each material are shown representing two experimental runs for each. All other data collected for films of these alloys exhibit the same general characteristics. Values calculated for $\tilde{K}'$ and $\tilde{K}$ are shown in Table I with the corresponding results for *a*-Bi of Naugle

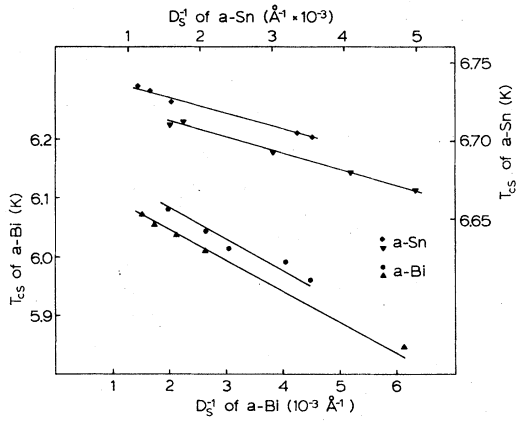

FIG. 2. Transition temperature of *a*-Bi and *a*-Sn films as a function of inverse film thickness.

et al.[17] and excellent agreement is observed.

Values determined for T_0 of *a*-Bi vary slightly between runs. In general, these values are distributed in the range from 6.10 to 6.19 K. Because the characteristic uncertainty in the transition temperature measurements is always less than 40 mK, these variations cannot be explained in terms of experimental error alone. Rather, it is more likely that these discrepancies reflect small changes in alloy composition due to distillation of one component from the source over a period of several runs. This view is supported by a general trend in the data which indicates that repeated use of the same source, without replenishment, results in successively lower values of T_0. Upon replenishment, however, measured values of T_0 are restored to near the top of the range.

The data for *a*-Sn films exhibit the same general behavior as observed in the *a*-Bi films. Values of T_0(6.66–6.72 K) for the *a*-Sn films are comparable to $T_c = 6.62$ K reported by Bergmann[12] for a 1620 Å

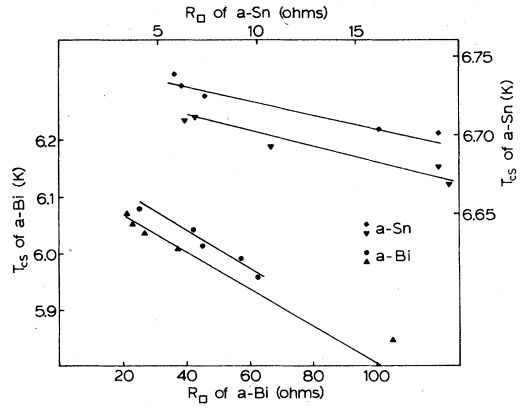

FIG. 3. Transition temperature of *a*-Bi and *a*-Sn films as a function of residual resistance per square.

TABLE I. Values of $\tilde{K}'$, $\tilde{K}$, and K for some amorphous superconductors.

Author	Material	$\tilde{K}'$ (K Å)	$\tilde{K}$ (K kΩ^{-1})	K (kΩ^{-1})
Naugle *et al.*[a]	*a*-Bi	62±9	3.9±0.6	0.63±0.05
This work	*a*-Bi	51±7	3.7±0.6	0.60±0.09
This work	*a*-Sn	11±3	2.8±0.8	0.41±0.15
Naugle *et al.*[a]	*a*-Pb	45±7	4.7±0.3	0.68±0.05
Naugle *et al.*[a]	*a*-Ga	22±5	6.8±1.3	0.80±0.15

[a]Reference 17.

amorphous film of the same alloy.

Naugle *et al.*[17] have noted an interesting property of the transition temperatures of films of *a*-Bi, amorphous lead (*a*-Pb) and amorphous gallium (*a*-Ga). Their results show a remarkable universality of behavior with respect to the value of the constant $K = \tilde{K}/T_0$. Values of K determined from this study are tabulated with that for these other amorphous superconductors in Table I. It is interesting to note that, within experimental error, this constant is the same for the four different amorphous superconductors.

B. Proximity effect

All proximity effect data gathered during the course of this study were analyzed according to the model of Eq. (11). The form of this expression, however, is not well suited to analysis since both parameters of interest (ξ_S and b) occur in the argument of the χ function. This complication is remedied by recasting Eq. (11) into a slightly different form by taking the inverse χ function, $\tilde{\chi}$, of each side. A slight rearrangement of terms then gives

$$D_S = \bar{\xi}_S X^{-1/2} - b \ , \tag{14}$$

where

$$X = 4t\tilde{\chi}(-\ln t)/\pi^2 \ , \tag{15}$$

$$\bar{\xi}_S = \xi_S / t^{1/2} \ , \tag{16}$$

and the reduced transition temperature t is defined to be T_c/T_{cS}.

The calculation of X is performed using the experimentally determined value of t for each sandwich. The calculation of $\tilde{\chi}$ is achieved by linearly interpolating the table of digamma functions in Ref. 13. The values of $\tilde{\chi}$ thus determined are estimated to be accurate to five significant figures.

The uncertainty $\delta(X^{-1/2})$ associated with the value of $X^{-1/2}$ is calculated numerically for each data point. This uncertainty never exceeds ±3%, thereby indicating that the uncertainty in the film thickness measurements should play the dominant role in the determination of $\bar{\xi}_S$ and b. For this reason, only thickness error bars are shown in the figures.

Figure 4 shows the proximity effect data plotted according to Eq. (14). The optimum values of $\bar{\xi}_S$ and b are determined from a weighted least-squares fit to the data and are shown in Table II. Values are also calculated for the pair penetration depth with $\rho_{Fe} = 1.11 \times 10^{-6}$ Ω m after Ref. 1. These results are also shown in Table II.

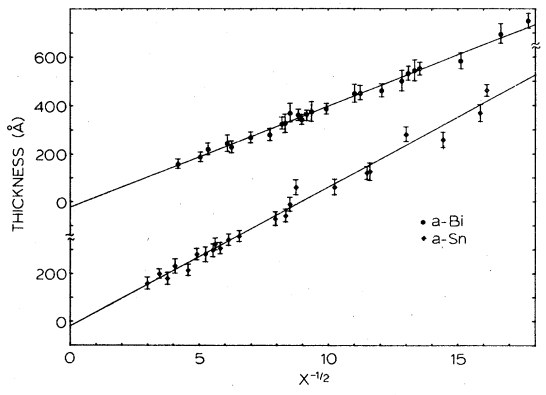

FIG. 4. S component thickness as a function of $X^{-1/2}$ for (*a*-Bi)-Fe and (*a*-Sn)-Fe proximity sandwiches.

TABLE II. Parameters characterizing proximity sandwiches with iron N component.

S component	$\bar{\xi}_S$ (Å)	b (Å)	k_N^{-1} (Å)
a-Bi	42±2	22±15	27±20
a-Sn	58±2	19±12	7±4

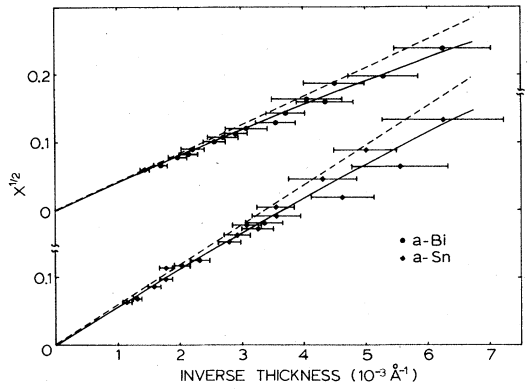

FIG. 5. The parameter $X^{1/2}$ as a function of inverse film thickness for (a-Bi)-Fe and (a-Sn)-Fe proximity sandwiches. The solid lines are drawn using $\bar{\xi}_S$ and b from Table II. Dashed lines are similarly constructed using $\bar{\xi}_S$ from Table II and $b = 0$.

In light of the large uncertainties associated with b and k_N^{-1} for each sandwich type, it is reasonable to question whether the data can be equally well described by the simpler model used by Lejeune and Naugle[5] which assumes that $b = 0$. To further illuminate this question, the data is plotted in the form $X^{1/2}$ vs D_S^{-1} in Fig. 5. In each case, the solid curve is calculated with values for $\bar{\xi}_S$ and b from Table II. The dashed line is calculated with the same value for $\bar{\xi}_S$ but with $b = 0$. In each case the data appear to be better described by the nonzero value of b which suggests that the values obtained for b and k_N^{-1} are significant.

Values of $\bar{\xi}_S$ for a-Bi and a-Sn as determined by other experiments are tabulated with the results of this work in Table III. With respect to the a-Bi results, the proximity effect study of Lejeune and Naugle[5] (LN) is most similar to this work, but the value of $\bar{\xi}_S$ reported is significantly larger. The principal difference between the experiments is that LN grew both sandwich components through the same mask; thus the S and N components were not separately resolvable, so that a method of independently determining one or the other was needed. LN accomplished this by mounting a glass slide on the bottom of the mask in such a way as to be exposed only during the Fe evaporation. An obvious defect in this procedure is that an additional measurement must be made to determine the thickness of the S component which introduces an additional ± 30 Å random error. The possibility of nonuniform vapor flux due to source characteristics could further increase the uncertainty in the value of D_S. Although we are unable to reproduce the filament geometry for the iron deposition used by LN, we now suspect that flux nonuniformity may have increased the LN thickness errors.

TABLE III. Values of $\bar{\xi}_S$ for a-Bi and a-Sn.

Author	Material	$\bar{\xi}_S$ (Å)
Lejeune and Naugle[a]	a-Bi	60 ± 4
Silverman[b]	a-Bi	63
Silverman[c]	a-Bi	46 ± 6
Bergmann[d]	a-Bi	44
This work	a-Bi	42 ± 2
Bergmann[d]	a-Sn	66
This work	a-Sn	58 ± 2

[a]Reference 5.
[b]Reference 10.
[c]Reference 11.
[d]Reference 12.

The errors associated with the thickness measurements in the present experiment have been at least halved from those of LN by the introduction of the dual mask deposition system. Also, the parameters $\bar{\xi}_S$ and b were determined by a fit for which the data points were weighted according to their uncertainties. Consequently we are considerably more confident in the thickness values and thus the values of $\bar{\xi}_S$ with this experiment.

The paraconductance experiments of Silverman were carried out under two different sets of conditions. The first set of measurements[10] was performed in the absence of magnetic field, whereas the second set[11] was performed in a perpendicular magnetic field. Each experiment produced a different value for $\bar{\xi}_S$. The larger value, resulting from the first experiment, required measurement of the associated film thickness for its determination. Although we are unaware of the details of the thickness measurements made by Silverman, it is interesting to note that Silverman, himself, in the latter work,[11] indicates that the thickness measurements may not be reliable. The thickness independent value reported in the later experiment, however, agrees well with this work, as can be seen from Table III.

Calculations of $\bar{\xi}_S$ made from measurements[12] of upper critical magnetic field (H_{c2}) as a function of temperature for a-Bi and a-Sn films provide additional corroboration for the results obtained from this study. In addition, these calculations provide the only comparison presently available for the a-Sn results.

Comparison of the results pertaining to the N component properties are complicated by the need to compare with other proximity effect experiments with the same components. This results from the fact that b is not solely a property of the N component but depends on the properties of the superconductor as well. The pair penetration depth, however, is deter-

mined only by the properties of the ferromagnetic material, as Eq. (9) indicates. Therefore, any proximity effect experiment which employs Fe as the N component should produce the same value of k_N^{-1}. The best we can say of the values of k_N^{-1} in Table II is that they are consistent within the rather large uncertainties. They are also consistent within the uncertainties with the value $k_N^{-1}=6$ Å given by Hauser *et al.*[1] but we do not believe that this comparison is significant since they estimated the value of ξ_N from the relation

$$\xi=(\pi\hbar k_B/6T_c e^2\rho\gamma)^{1/2} ,$$

where γ is the Sommerfeld constant. This expression is equivalent to Eq. (5) of Sec. II. In addition to the fact that the uncertainties propagated through the calculation of ξ_N can become quite large, the value of γ_{Fe} used corresponds to crystalline iron. This value is quite likely inappropriate for the microcrystalline or amorphous Fe which comprises the N component of the sandwiches.

It should be noted that good values of the coherence length can be obtained for relatively thick films ($D_S \geq 10\bar{\xi}_S$) with $b=0$. Furthermore, the values of both b and k_N^{-1} are less than the mean thickness required for film continuity which should approximate the peak-to-peak surface roughness. Thus, the physical interpretation of the fitted value of b is perhaps not as straightforward as the theory would indicate.

V. SUMMARY AND CONCLUSIONS

These proximity effect experiments have resolved the controversy over the value of the coherence length for a-Bi. The preponderance of evidence now indicates it should be $\bar{\xi}_S=42\pm2$ Å. They also support the HTW theory of proximity effect with a magnetic normal metal.

The measurements of T_{cS} as a function of $R_\square$ may be described by Eq. (13) where $K=\tilde{K}/T_0$ is essentially the same constant for the four amorphous superconductors for which such data is available. To date there is no theoretical justification for this apparent universal behavior.

ACKNOWLEDGMENTS

This research was supported in part by the National Science Foundation and the Robert A. Welch Foundation. G. Cort was the grateful recipient of a Robert A. Welch Pre-Doctoral Fellowship during much of this work.

*Present address: Los Alamos Scientific Laboratory, Los Alamos, N.M. 87545.

[1] J. J. Hauser, H. C. Theuerer and N. R. Werthamer, Phys. Rev. 142, 118 (1966).
[2] C. J. Kircher, Phys. Rev. 168, 437 (1968).
[3] R. O. Smith, W. L. McLean, and B. Serin, J. Low Temp. Phys. 4, 317 (1971).
[4] J. J. Hauser, Phys. Rev. B 10, 2792 (1974).
[5] J. D. Lejeune and D. G. Naugle, in *Proceedings of the Fourteenth International Conference on Low Temperature Physics,* edited by M. Krusius and M. Vuorio (North-Holland, New York, 1976), pp. 269–272.
[6] J. J. Hauser, N. R. Werthamer, R. O. Smith, W. L. McLean, and B. Serin, J. Low Temp. Phys. 8, 171 (1972).
[7] P. G. de Gennes and E. Guyon, Phys. Lett. 3, 168 (1963).
[8] N. R. Werthamer, Phys. Rev. 132, 2440 (1963).
[9] P. G. de Gennes, Rev. Mod. Phys. 36, 225 (1964).
[10] P. J. Silverman, Phys. Rev. B 16, 2066 (1977).
[11] P. J. Silverman, Phys. Rev. B 19, 233 (1979).
[12] G. Bergmann, Phys. Rev. B 7, 4850 (1973).
[13] P. J. Davis, in *Handbook of Mathematical Functions with Formulas, Graphs and Tables,* edited by Milton Abramowitz and Irene A. Stegun (U.S. Department of Commerce, Washington, D.C., 1964), pp. 253–270.
[14] A. C. Rose-Innes and B. Serin, Phys. Rev. Lett. 7, 278 (1961).
[15] D. G. Naugle, J. W. Baker, and R. E. Allen, Phys. Rev. 7, 3028 (1973).
[16] W. Buckel and R. Hilsch, Z. Phys. 138, 109 (1954).
[17] D. G. Naugle, R. E. Glover, III, and W. Moormann, Physica (Utrecht) 55, 250 (1971).
[18] R. E. Glover, III, Physica (Utrecht) 55, 3 (1971).
[19] J. D. Lejeune, D. G. Naugle, and J. W. Baker, J. Appl. Phys. 45, 5043 (1974).
[20] D. Korn, H. Pfeifle, and G. Zibold, Z. Phys. 270, 195 (1974).
[21] D. Korn, W. Muerer, and G. Zibold, Phys. Lett. 47A, 117 (1974).
[22] V. Buck, Z. Phys. 270, 209 (1974).
[23] G. Bergmann, Phys. Rep. 27C, 159 (1976).
[24] S. Tolansky, Nature (London) 153, 413 (1944).